ANALYSIS OF OSB MAT STUCTURE MADE FROM INDUSTRIALLY MANUFACTURED STRANDS USING SIMULATION MODELING

Jeroen H. van Houts

Post-Doctoral Research Associate
Tennessee Forest Products Center
Department of of Forestry, Wildlife and Fisheries
The University of Tennessee
Knoxville, TN 37996-4570

Paul M. Winistorfer†

Professor and Department Head
Department of Wood Science and Forest Products
Virginia Tech
Blacksburg, VA 24061-0323

and

Siqun Wang†

Assistant Professor
Tennessee Forest Products Center
Department of Forestry, Wildlife and Fisheries
The University of Tennessee
Knoxville, TN 37996-4570

(Received June 2001)

ABSTRACT

Industrially manufactured oriented strandboard (OSB) furnish was characterized by scanning images of a large number of individual strands and analyzing their shape properties. A Visual Basic macro in combination with commercially available image synthesis software was utilized to carry out the task of this analysis. The scanned images of these strands were used in a model that simulates the formation of layers within an OSB mat. These layers were simulated using three different orientation scenarios: random orientation. 100% strand alignment, and strand alignment based on industrial parameters. Information provided by the model includes the number and geometrical details of voids and strand overlap. Totat void area for a mat is shown to be independant of strand orientation and the aspect ratio of strands. Interestingly, noticeable differences in the number, size, orientation, and shape factor of the individual voids, which make up the total area, were shown between various mat configurations.

Keywords: Simulation model, OSB, slenderness ratio, voids, strand overlap, mat structure, dimensional stability.

INTRODUCTION

Because of the nature of the strands and the mat formation process, OSB has a notable horizontal density distribution that is largely dominated by variation in the number of overlapping strands at any given point through the mat thickness and the presence of voids (Lu and Lam 1999; Dai and Steiner 1997; Xu and Steiner 1995; Oudjehane and Lam 1998; Suchsland and Xu 1989). Similarly, a discrete layer of strands will have a horizontal density distribution (due to variations in the number of overlapping strands) and also, if the weight of the layer is low, there will be a tendency for areas to contain no strands at all (i.e., lim-

† Member of SWST.

Wood and Fiber Science, 35(3), 2003, pp. 351–362

ited or minimal surface area coverage). Strand characteristics and the mat forming process will define the distribution and number of overlapping strands and also the uncovered areas within a given layer.

With the use of a simulation model, the influence of a number of parameters on the area coverage characteristics of a discrete layer of strands is reported. The results from this investigation will better help to define the amount of furnish required to form a layer providing a certain degree of strand coverage (i.e., knowledge of strand coverage versus void area), and will also establish whether the addressed parameters can be manipulated in such a way as to produce a panel with more uniform strand coverage.

Three major parameters, namely strand geometry, strand orientation, and strand location, must be addressed when modeling mat structure. Methodologies that have been used to incorporate these parameters in models by previous researchers are discussed, and comparisons are made with the simulation model presented herein.

Strand geometry

To date, the most common strand geometry used for computer simulation of mat formation of OSB or flakeboard has been rectangular. Steiner and Dai (1993) and Dai and Steiner (1994a, b) developed a Monte Carlo simulation technique that allowed a mat to be modeled by simulating the placement of rectangular strands at random locations and random orientations within a given area. Later, Lu et al. (1998), Oudjehane et al. (1998a, b), and Oudjehane and Lam (1998) further developed models based on the same simulation techniques used by Dai and Steiner (1994a, b). These models explored further mat formation parameters such as the influence of flake dimensions, flake orientation, and the fixed and random positioning of flake centers. Yet the similarity between all of these simulation models has been the use of perfectly rectangular flakes.

The original model (Steiner and Dai 1993; Dai and Steiner 1994a, b) has been extended since it was initially developed. Some information has been published discussing the development of a model that takes into account variations in strand shape based on observations of industrial strand geometry (Dai and Chen 1996) and even including the presence of fines in a future simulation package (Dai et al. 1997). Chen et al. (1998) introduced the use of an image analysis system to measure strand length, width, and shape of commercial strand samples. The strand shapes were classified into five representative groups and, along with the length and width data, frequency distributions of this information were generated. It appears that the strands used to model a mat were generated from the distribution data. Interestingly, fines were considered as a separate entity from the strands, and were assumed to be of random size and shape. Specific information on the distributions of strand (or fine) shapes and sizes was not reported.

Our modeling work was partially based on materials published by the authors mentioned above, with a number of differences in how some of the governing parameters were applied and the results sought. The simulation model utilizes the actual images of commercial strands and also smaller particles including broken strands and fines. This has obvious advantages over simply using rectangular-shaped strands, and provides a more realistic representation than using selected shapes to which the strands have been classified. A disadvantage, however, is that the enhanced realism of using the images of real strands requires significantly greater computational time than would be applicable when using much simpler geometric shapes.

Strand orientation

Strand orientation in OSB is known to affect a number of panel properties such as MOE and MOR (Barnes 2000), and linear expansion (Xu 2000). Previous models have investigated the influence of strand orientation

by using a number of techniques. These techniques have primarily been random orientation (Dai and Steiner 1994a; Lu et al. 1998; Oudjehane et al. 1998a, b), orientation defined by a normal distribution (Chen et al. 1998; Lau 1981), orientation defined by the von Mises distribution (Shaler and Blankenhorn 1990), and fixed orientation (Oudjehane and Lam 1998; Lu and Lam 1999).

Three levels of orientation were investigated in our research using the simulation model, including random orientation, industrial orientation, and 100% orientation. Random orientation and 100% orientation were applied in a manner independent of individual strand properties, while industrial orientation utilized dimensional properties of each strand in order to define a field in which it was randomly placed.

Strand location

Different approaches have been used for modeling the location of strand centers. Generally, these have either been random (Dai and Steiner 1994a) or fixed position (Oudjehane and Lam 1998; Oudjehane et al. 1998a, b). Variations of the deposition process have included locating fines according to density distribution in order to reflect the fact that fines tend to move to voids or low density areas (Chen et al. 1998).

Some of the previous modeling work has been validated using panels constructed with the aid of a robot (Lu and Lam 1999; Lu et al. 1998; Oudjehane et al. 1998a, b; Wang and Lam 1998). The robot is capable of placing individual strands at a predetermined location and orientation, hence allowing a panel to be produced that is very similar to the panel described by a model. Properties such as horizontal density distribution and modulus of elasticity have been predicted with a model and then compared with the empirical data from robot-formed panels.

In all cases presented herein, the simulation model assumed random positioning of the strands. However, if there was a future requirement for the model to position strands in a non- or partially-random fashion, possibly even dependent on individual strand properties, modification of the simulation model would be relatively simple to allow for this.

MATERIALS AND METHODS

Commercially produced southern pine strands, which had been manufactured with a target length of 102 mm and thickness of 0.7 mm, and an uncontrolled width dimension, were utilized for this research. A flat bed scanner had been previously used to analyze the strand coverage of discrete layers within a mat, and the size of the simulated panel was based on the scanner bed dimensions (224 $\times$ 367 mm). This same simulated panel size was used as a basis for calculating the amount of strands used in this study also.

This study was based on discrete layers within a 12.7-mm-thick panel with an average density of 473 kg/m^3. The sizes of the discrete layers investigated were 12.5% and 25% of the total mat weight (dry basis), which correspond to the same discrete layer size in the previous experimental investigation (van Houts et al. 2003).

Strand characterization

Four samples of strands, each with a dry weight representing 4.17% (20.57 g) of the total weight of the simulated panel size, were randomly selected. These samples of strands included a range of different-sized particles including whole strands, broken strands, and fines. Each of these particles (which will herein be referred to as strands regardless of size) was scanned individually on a flat bed scanner to produce grayscale images with a resolution of 5.86 pixels per mm of the original size. Care was taken to scan each strand with the same orientation, resulting in all the images being oriented with their length dimension in the vertical direction (as viewed on the computer screen).

A commercial image analysis software package, SigmaScan® Pro 5.0 (1999), was used to analyze various properties of the

strand images. A Visual Basic macro was written in order to automate the process of obtaining and saving data for all the strand images. The information collected includes strand area, major and minor axis length, and shape factor. Major axis length can be defined as the distance between the two farthest apart points on a strand. Minor axis length is measured perpendicular to the major axis and is the distance between the two farthest apart points in that direction. Shape factor is a measure of roundness of a strand image and can be represented by the following equation:

$$\text{shape factor} = \frac{4\pi a}{p^2} \qquad (1)$$

where a is the strand area and p is the length of the perimeter around the strand. A perfect circle would therefore have a shape factor of 1 while a line has a shape factor approaching 0. Calculation of shape factor was a feature of the image analysis software which, in addition to the major and minor axis length, gave an indication of whether a strand had a high length to width ratio.

Modeling mat layers

The scanned images of the strands were used to model the formation of discrete layers within OSB. SigmaScan® Pro 5.0 (1999) was the platform for this model, with a Visual Basic macro that controlled all of the required functions. The main procedures carried out by the model are outlined below:

1. Open a strand image file.
2. Manipulate the brightness of the grayscale image to produce a pure white strand (intensity 255) on a pure black background (intensity 0).
3. Reduce the image brightness such that the strand has an intensity of 1 and the background intensity remains at 0.
4. Orientate the image as required.
5. Add this image, with its center at a random location, onto a blank image (with black background). The blank image is the size of the simulated panel, which was chosen to be the same size as the scanner bed. If part of the strand image protrudes from the edge of the blank image, then the ''torus convention'' concept is applied (described below).
6. Repeat steps 1 to 5, while still adding the images to the same black image until the desired mat weight per unit area has been reached. Note that a single strand appearing on the blank image has an intensity of 1; however, as more strands are added to this blank image, they will begin to overlap. At a point where two or more strands overlap, the intensity will be equal to the number of overlapping strands, until this number reaches a maximum of 255 (pure white).
7. The ''blank image'' is analyzed using object detection functions to determine information such as the distribution of overlapping strands, and the size, shape factor, and orientation of voids.

The ''torus convention'' concept (Hall 1988) referred to in step 5 has previously been used when modeling strand mats in cases where the ''edge effect'' is not considered (Dai and Steiner 1994a; Lu et al. 1998). Because the center of the strand image is placed randomly on the blank image, there are times when part of a strand may not be inside the blank image. The ''torus convention'' dictates that the part of the strand protruding from the blank image again enters from the opposite side. This has a similar effect as the simulated mat being considered as part of a large mat.

The above procedure was followed for a number of different mat configurations. These different configurations involved varying the layer weight (12.5% or 25%), furnish orientation (random, 100% orientation, or simulated industrial orientation), and strand geometry (normal, high slenderness ratio, or low slenderness ratio).

The strand images were stored in separate folders, with each folder containing strands for a 4.17% layer (by weight) within the mat. For a 12.5% layer, the model would use the contents of three of these folders. However, be-

cause only four folders existed for each furnish type, the images in two of the folders were used twice when a 25% layer was modeled as the contents of six folders was required.

It should be noted that the modeling technique does not include the consolidation of the mat and does not consider any redistribution of mass and structure that occurs during this process. However, during consolidation, the major component of strand relocation occurs in the thickness direction. The model is two-dimensional and does not consider the through-thickness direction and therefore has some validity for analysis of a consolidated panel.

Strand orientation was relatively simple to control for two of the three different scenarios. Using the Visual Basic macro to randomly generate a number from 0 to 1, and multiplying it by 360° achieved a value for random orientation that was applied to a strand before being placed on the blank image. An orientation of 100% was achieved by not carrying out any re-orientation of the images, which had already been scanned in an oriented manner. The third and somewhat more involved orienting technique was termed ''industrial orientation,'' as it was designed to mimic the orientation that may be achieved in a disc type orienter. The basic principle for this type of orienter is that strands must fall between rotating discs. The strand dimensions, distance between the discs, and the distance that the strands fall from the orienter to the mat therefore primarily influence orientation. This concept dictates that longer strands are more highly oriented than short strands, which may not be oriented at all if their length is less than the distance between the discs.

Industrial orientation was achieved by considering the length of the major axis of the strand (L_M) and the distance between the orienter discs (D), assumed to be 38 mm. With this information, geometric constraints were considered when defining the limit of orientation for a strand when it passed between orienter discs. An assumption was made that the major axis of each strand remains horizontal as it falls between the discs. Also, it was assumed that strands might fall between the discs either on their edge or lying flat (i.e., the minor axis can be oriented in any direction). If the distance between the orienter discs was greater than L_M, then a strand was considered randomly oriented; otherwise limits of orientation were calculated from:

$$\text{orientation limit} = \sin^{-1}\left(\frac{D}{L_M}\right) \times C_{FF} \quad (2)$$

where C_{FF} is a coefficient that allows for further orientation change of the strand as it free-falls from the orienter to the mat surface. This equation was derived from the geometric constraints of positioning a strand between two orienter discs while assuming that the major axis of the strand remains horizontal. For the model run, the chosen value of C_{FF} was 1.1 (this value indicates that the orientation of a strand may change by 10% while it free-falls from the orienter discs to the mat surface). After calculation of the orientation limit for a strand, this value was multiplied by a randomly generated number between -1 and 1, and then used as the orientation for the strand. Orientation values generated using this technique were compared to previously published information on strand orientation.

Three different strand geometries were considered to identify their influence on mat structure. Normal strand geometry was when the originally scanned images were used in the model. High slenderness ratio was achieved by manipulating each strand image in such a way as to stretch it so that the length of the strand increased by 50% and the width decreased appropriately to maintain the same strand area. Low slenderness ratio was achieved by reducing the length of each strand by 50% and increasing its width in order to maintain its original area.

Data generated by the model were imported into a spreadsheet where they were converted into a number of different graphs for comparison purposes.

TABLE 1. *Summary of strand characteristics (note that each batch represents 20.57 g of strand material).*

	Strand batch code				All strands
	U1	U2	U3	U4	
Number of strands	118	70	107	70	365
Average area (mm^2)	630	909	703	912	759
Total area (mm^2)	74,340	63,630	75,221	63,840	277,035
Average shape factor	0.169	0.179	0.164	0.170	0.170
Average major axis length (mm)	75.8	83.7	80.4	82.1	79.9
Average minor axis length (mm)	9.4	12.3	9.8	11.7	10.5

RESULTS AND DISCUSSION

Strand characterization

A summary of the average area, total area, shape factor, major axis length, and minor axis length for the strands is shown in Table 1. The total area of a given batch was found by multiplying the number of strands by the average area. This total area value gives an indication of the coverage potential for each batch of strands. If the strands were all of equal thickness and the same density, the total area would be equal for each batch.

Figures 1, 2, 3, and 4 show the area, shape factor, major axis length, and minor axis length distributions of all the strands, respectively. Several pieces of information can be extracted from these distributions. A large portion of the strands are under the target length (102 mm), and the vast majority of the strands have a width under 15 mm. These strand characterization techniques would be useful for comparing geometric attributes of strands from different sources, or even providing a guide for checking the performance of strand manufacturing equipment.

Modeling mat layers

For each different configuration, the simulation model was run 20 times using the same strands, and whenever possible the average and standard deviation values for the data were calculated. Figures 5 and 6 display coverage characteristics for 12.5% and 25% layers, respectively, of randomly and 100% oriented normal slenderness ratio strands, in a 12.7-mm-thick panel with an average density of 473 kg/m^3. By comparing these two figures, the influence of the amount of furnish in a

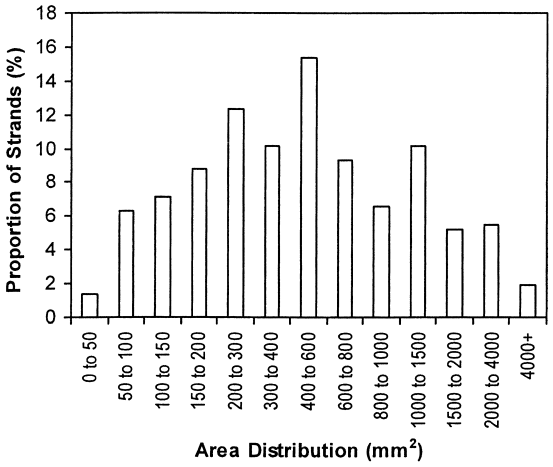

FIG. 1. Distribution of area for the scanned strands.

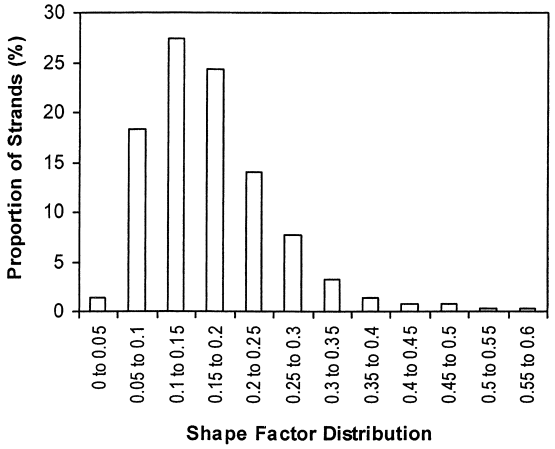

FIG. 2. Distribution of shape factor for the scanned strands.

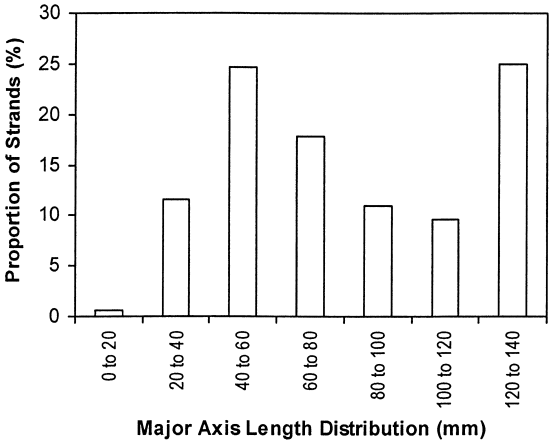

FIG. 3. Distribution of major axis length for the scanned strands.

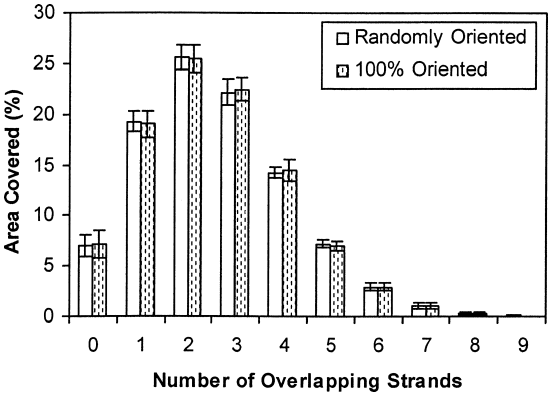

FIG. 5. Area covered by different numbers of overlapping strands in a 12.5% layer (normal slenderness ratio strands). Note that the error bars indicate one standard deviation from the mean.

layer is quite apparent. The 12.5% layer of strands in Fig. 5 shows an uncovered area (0 strands) of approximately 7%, while the 25% layer of strands shown in Fig. 6 has an uncovered area of less than 1%. Also, the 25% layer of strands has higher numbers of overlapping strands than in the 12.5% layer, which is logical considering that a higher number of strands are present.

From Figs. 5 and 6, orientation does not appear to influence the amount of area covered by a given type of strand for a given layer thickness. When the model was run using industrial orientation, or other strand geometries, such as high slenderness ratio, or low slenderness ratio, the proportions of area covered by various numbers of strands did not change. However, these factors were found to influence the size distribution, shape, and orientation of voids (areas with no strands).

All of the normal slenderness ratio strands were oriented 100,000 times using the industrial orientation routine and each generated angle was recorded. The distribution of these angles was calculated at 1-degree intervals, normalized, and is presented in Fig. 7. The orientation of strands can be defined by an

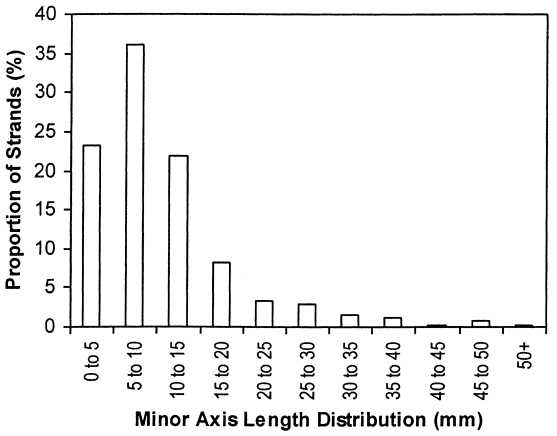

FIG. 4. Distribution of minor axis length for the scanned strands.

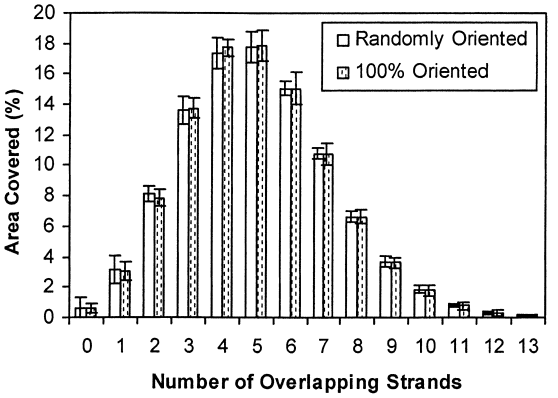

FIG. 6. Area covered by different numbers of overlapping strands in a 25% layer (normal slenderness ratio strands). Note that the error bars indicate one standard deviation from the mean.

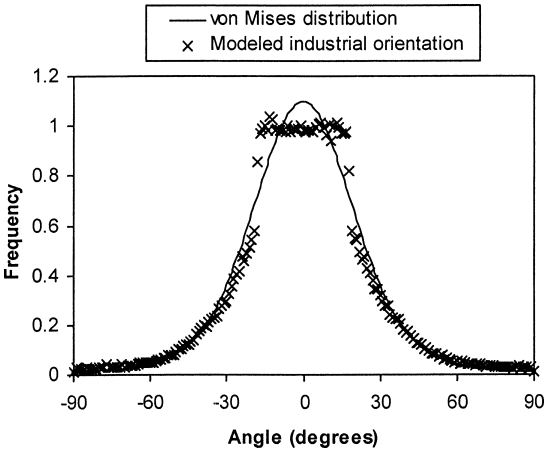

FIG. 7. Orientation distribution of normal slenderness ratio strands as modeled for an industrial production scenario compared with the von Mises distribution (κ = 2.22).

alignment calculation as introduced by Geimer (1976):

$$\text{align } \% = \frac{45 - \theta}{45} \times 100 \qquad (3)$$

where

$$\theta = \frac{\sum |\text{strand angles}|}{\text{sample size}} \qquad (4)$$

Alternatively, the von Mises distribution, which has been previously used to define strand alignment by Shaler (1991), Harris and Johnson (1982), Shaler and Blankenhorn (1990), and Wu (1999) can be used. The functional form of the von Mises probability density function is:

$$g(\theta;\, \mu_0,\, \kappa) = \frac{1}{\pi I_0(\kappa)} e^{\kappa \cos 2(\theta - \mu_0)} \qquad (5)$$

where θ is the angle (in radians), κ is the concentration parameter, μ is the mean angle, and $I_0(\kappa)$ is the modified Bessel function of order zero. Further information regarding the von Mises probability density function including a description of the modified Bessel function can be found in Harris and Johnson (1982).

When the alignment calculation was applied to the 100,000 angles that were generated using the industrial orientation technique, the percentage alignment was found to be 58%. A least squares method was used to fit the von Mises probability density function to the orientation distribution generated by the model and is shown in Fig. 7. The concentration parameter (κ) of the von Mises probability density function was found to be 2.22 with an r-square fit to the industrial orientation results of 0.97. Interestingly, the modeled industrial orientation angular distribution has a ''flat'' region that extends from approximately $-15°$ to $15°$. This characteristic of the distribution is a result of the assumptions made regarding the effect of distance between orienter discs and flake dimensions. According to the applied industrial orientation technique, the length of this flat region in the distribution would increase as the distance between orienter discs increases. Whether this phenomenon occurs in industrially manufactured panels is unknown to the authors.

For the discussion of results herein, voids have been defined as any area of the modeled mat layer that is not covered by at least one strand. It is accepted that voids certainly exist that have been covered by strands before a layer is compacted, and some of these voids will remain after compaction, but because of the two-dimensional nature of this model, these types of voids cannot be readily identified. However, it is believed that the voids as defined in the model (uncovered areas) are representative in shape and size of the voids that have been covered by strands in a layer.

Table 2 provides a summary of the shape factor of voids larger than 10 mm^2 from a number of different strand and orientation configurations as predicted by the simulation model. Small voids were not considered for calculating the average shape factor because they made up only a small portion of the total void area and, when included, resulted in an average value that was not representative. The influence of orientation is clear in that the shape factor of the voids decreases as the degree of strand orientation increases. This

TABLE 2. *Average void shape factors for voids larger than 10 mm.*[2]

	Random orientation	Industrial orientation	100% oriented
12.5% Layer			
Normal slenderness ratio	0.38 (0.14)*	0.26 (0.11)	0.16 (0.10)
High slenderness ratio	0.42 (0.14)	—	0.12 (0.09)
Low slenderness ratio	0.31 (0.12)	—	0.24 (0.13)
25% Layer			
Normal slenderness ratio	0.42 (0.13)	0.29 (0.12)	0.18 (0.10)
High slenderness ratio	0.45 (0.14)	—	0.16 (0.10)
Low slenderness raio	0.35 (0.11)	—	0.26 (0.11)

* Standard deviation is shown in parentheses.

stands to reason, as in a highly oriented mat layer the edges of adjacent strands are generally near parallel to each other, and hence spaces between strands would typically be long and narrow in shape.

The results presented in Table 2 clearly suggest some degree of interaction between the slenderness ratio of the strands and their orientation. In the randomly oriented mat layer configuration, low slenderness ratio strands have a void shape factor lower than the normal strands, while the high slenderness strands have a similar void shape factor to the normal strands. In the 100% oriented mat layers, the void shape factor decreases for all strand slenderness ratios; however, this decrease in shape factor is most significant for the high slenderness ratio strands and least significant for the low slenderness ratio strands.

For a 25% (by weight) mat layer, distributions of the major axis orientation of voids over 10 mm^2 for random, industrial, and 100% orientation configurations of normal slenderness ratio strands are shown in Fig. 8. Voids in the mat of randomly orientated strands were randomly orientated while void orientation increased as strand alignment increased, as shown for the 100% and industrially oriented mats.

Lenth and Kamke (1996) studied void characteristics on the edge of flakeboard mats, and concluded that flake orientation did not significantly influence void size, but did affect void shape. The edge of mats with flakes perpendicular to its plane consisted of shorter thicker voids (higher shape factor), while the perpendicular edge, with flakes parallel to its plane had thinner voids (lower shape factor). Randomly oriented flake mats had voids on their edges with an average shape factor intermediate to those of the aligned mats. These results compare well with the void structures seen in the plane parallel to the surface of the strand mat investigated using the simulation model.

Figures 9, 10, and 11 display the cumulative void area as a function of individual void size for randomly oriented, industrially oriented, and 100% oriented 25% (by weight) mat layers, respectively (normal slenderness ratio strands). All of the data from 20 modeled layers are represented in each figure to demonstrate the variation in results. It has already been indicated that the average total uncovered area (all of the voids added together) is the same regardless of strand orientation; however, Figs. 9, l0, and 11 indicate that the distribution of void sizes varies with orientation. With increased orientation, there is a tendency for fewer small voids and a greater number of large voids to be present (i.e., the slope of these graphs decreases with increased orientation). The void size distribution of the same mats prepared with the long slenderness ratio strands displayed very similar results to those mats formed from the normal slenderness ratio strands. Mats modeled from the short slenderness ratio strands did not show significant dif-

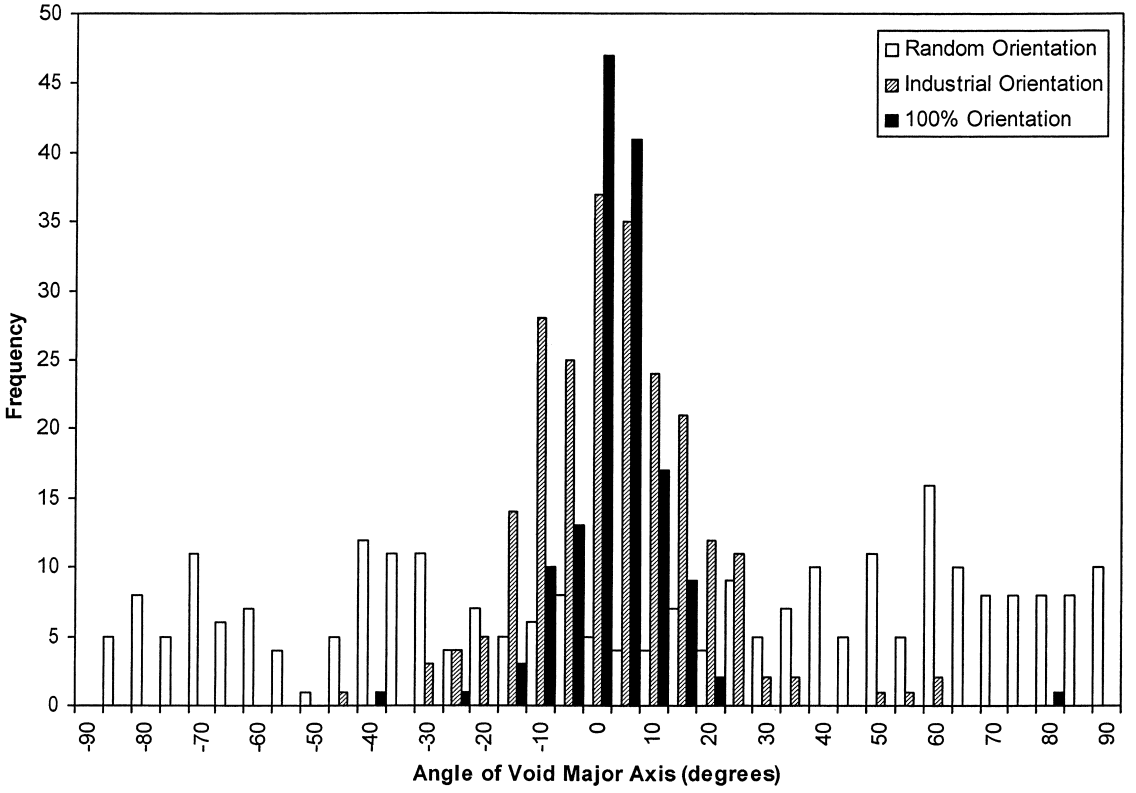

FIG. 8. Distribution of void major axis orientation for simulated 25% mat layers using normal slenderness ratio strands in random, industrial and 100% orientation configurations.

ferences in void size distribution when strand orientation was varied; when the slenderness ratio of a strand is decreased, its shape becomes somewhat closer to a square or even circular geometry. For these types of geometry, the influence of orientation has significantly less bearing on coverage characteristics than for elements of an elongated nature.

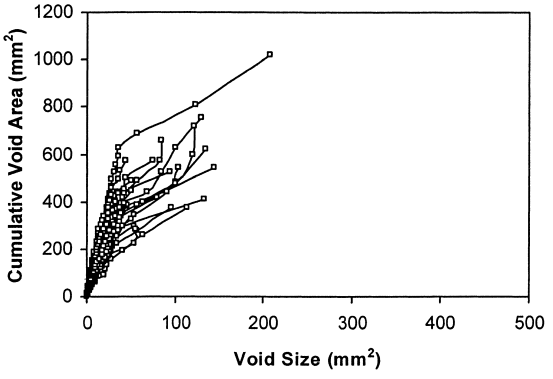

FIG. 9. Cumulative void size as a function of void size for 25% layer of randomly oriented normal slenderness ratio strands.

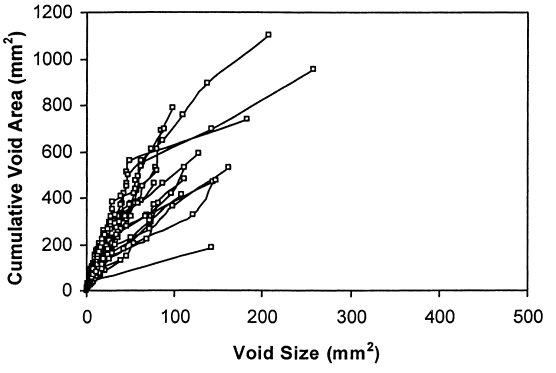

FIG. 10. Cumulative void size as a function of void size for 25% layer of industrially oriented normal slenderness ratio strands.

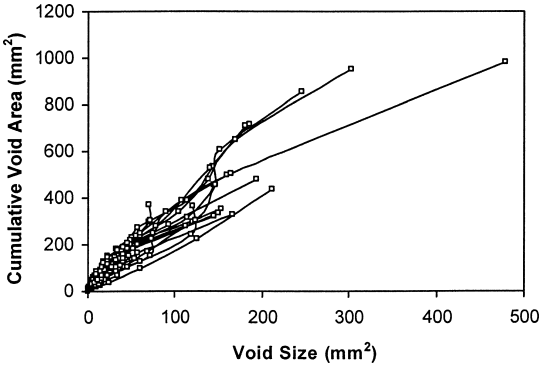

FIG. 11. Cumulative void size as a function of void size for 25% layer of 100% oriented normal slenderness ratio strands.

CONCLUSIONS

The strand characterization methodology presented in this article allows the determination of strand area, shape factor, major axis length, and minor axis length distribution. This could be utilized as a useful tool to compare furnish from different processes, and as a technique for assessing the performance of strand manufacturing equipment.

Results from the simulation model have provided much information regarding mat layer coverage characteristics when using scanned images of industrially procured strands. The information from this modeling exercise is invaluable when interpreting the coverage potential of a given amount of furnish, and also provides significant information on the voids present within a given mat structure. The actual total area covered by various numbers of overlapping strands or voids was found to be dependent on the amount of furnish present, not on orientation or slenderness ratio. The distribution of void size, shape factor, and orientation, however, was found to be dependent on both strand orientation and slenderness ratio.

ACKNOWLEDGMENTS

This work was supported by USDA Special Grant R11-2218-54 and partly supported by the Tennessee Agricultural Experiment Station, Projects MS76 and MS83. The authors would like to thank J. M. Huber for providing experimental materials.

REFERENCES

BARNES, D. 2000. An integrated model of the effect of processing parameters on the strength properties of oriented strand wood products. Forest Prod. J. 50(11/12): 33–42.

CHEN, S., P. HUBERT, AND C. DAI. 1998. Process modeling for wood-based composites. Part I. Computer simulation for OSB mat formation. Pages 31–35 *in* Engineering Systems Using Structural Panels. Proc. 7272, Forest Products Society, Madison, WI.

DAI, C., AND S. CHEN. 1996. Simulation of mat formation for wood strand composite processing. Pages 32–39 *in* H. Kajita and K. Tsunoda, eds. Proc. Third Pacific Rim Bio-Based Composites Symposium, Kyoto, Japan.

———, AND P. R. STEINER. 1994a. Spatial structure of wood composites in relation to processing and performance characteristics. Part 2. Modelling and simulation of a randomly-formed flake layer network. Wood Sci. Technol. 28(2):135–146.

———, AND ———. 1994b. Spatial structure of wood composites in relation to processing and performance characteristics. Part 3. Modelling the formation of multi-layered random flake mats. Wood Sci. Technol. 28(3): 229–239.

———, AND ———. 1997. On horizontal density variation in randomly-formed short-fibre wood composite boards. Composites Part A, 28A:57–64.

———, P. HUBERT, AND CHEN. 1997. Advances in modeling mat formation and consolidation for wood composite panels. Pages 21–27 *in* J. Hague, C. Loxton, J. Bolton, and L. Mott, eds. Proc. First European Panel Products Symposium, Llandudno, Wales.

GEIMER, R. L. 1976. Flake alignment in particleboard as affected by machine variables and particle geometry. Res. Paper FPL 275, USDA, Forest Prod. Lab., Madison, WI. 16 pp.

HALL, P. 1988. Introduction to the theory of coverage processes. John Wiley and Sons, New York, NY. 408 pp.

HARRIS, R. A., AND J. A. JOHNSON. 1982. Characterization of the flake orientation in flakeboard by the von Mises probability distribution function. Wood Fiber 14(4): 254–266.

LAU, P. W. C. 1981. Numerical approach to predict the modulus of elasticity of oriented waferboard. Wood Science 14(2):73–85.

LENTH, C. A., AND F. A. KAMKE. 1996. Investigations of flakeboard mat consolidation. Part I. Characterizing the cellular structure. Wood Fiber Sci. 28(2):153–167.

LU, C., AND F. LAM. 1999. Study on the X-ray calibration and overlap measurements in robot-formed flakeboard mats. Wood Sci. Technol. 33(2):85–95.

———, P. R. STEINER, AND F. LAM. 1998. Simulation

study of wood-flake composite mat structures. Forest Prod. J. 48(5):89–93.

OUDJEHANE, A., AND F. LAM. 1998. On the density profile within random and oriented wood-based composite panels: Horizontal distribution. Composites Part B, 29B: 687–694.

———, ———, AND S. AVRAMIDIS. 1998a. Forming and pressing processes of random and oriented wood composite mats. Composites Part B, 29B:211–215.

———, ———, AND ———. 1998b. Modeling the influence of the formation process on engineering properties of flakeboards. Pages 1–5 *in* Engineering Systems Using Structural Panels. Proc. 7272, Forest Products Society, Madison, WI.

SHALER, S. M. 1991. Comparing two measures of flake alignment. Wood Sci. Technol. 26(1):53–61.

———, AND P. R. BLANKENHORN. 1990. Composite model prediction of elastic moduli for flakeboard. Wood Fiber Sci. 22(3):246–261.

SigmaScan® Pro 5.0. 1999. SigmaScan® Pro. 5.0 User's Guide. SPSS Inc., Chicago, IL. 281 pp.

STEINER, P. R., AND C. DAI. 1993. Spatial structure of wood composites in relation to processing and performance characteristics. Part I. Rationale for model development. Wood Sci. Technol. 28(1):45–51.

SUCHSLAND, O., AND H. XU. 1989. A simulation of the horizontal density distribution in a flakeboard. Forest Prod. J. 39(5):29–33.

VAN HOUTS, J. H., P. M. WINISTORFER, AND S. WANG. 2003. Improving dimensional stability by acetylation of discrete layers within oriented strandboard. Forest Prod. J. 53(1):82–88.

WANG, K., AND F. LAM. 1998. Robot-based research on three-layer oriented flakeboards. Wood Fiber Sci. 30(4): 339–347.

WU, Q. 1999. In-plane dimensional stability of oriented strand panel: Effect of processing variables. Wood Fiber Sci. 31(1):28–40.

XU, W. 2000. Influence of percent alignment and shelling ration on linear expansion of oriented strandboard: A model investigation. Forest Prod. J. 50(7/8):88–93.

———, AND P. R. STEINER. 1995. A statistical characterization of the horizontal density distribution in flakeboard. Wood Fiber Sci. 27(2):160–167.